2nd Advanced Optical Metrology Compendium

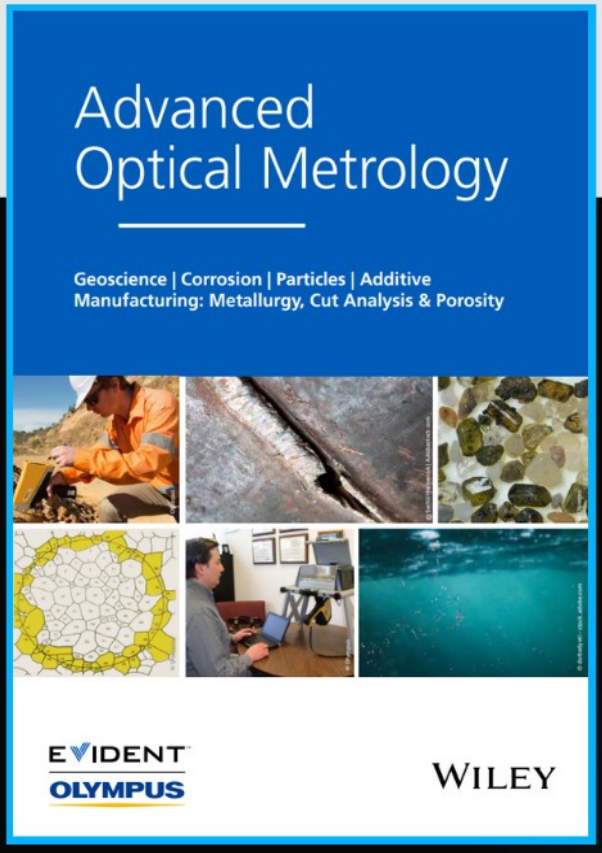

The latest eBook from Advanced Optical Metrology. Download for free.

This compendium includes a collection of optical metrology papers, a repository of teaching materials, and instructions on how to publish scientific achievements.

With the aim of improving communication between fundamental research and industrial applications in the field of optical metrology we have collected and organized existing information and made it more accessible and useful for researchers and practitioners.

EVIDENT™
OLYMPUS

WILEY

NANO MICRO small

High Payload Dual Therapeutic-Imaging Nanocarriers for Triggered Tumor Delivery

*Jin-Ki Kim, Hong Yuan, Jingxin Nie, Yu-Tsai Yang, Markos Leggas, Philip M. Potter, John Rinehart, Michael Jay, and Xiuling Lu**

The in vitro *and* in vivo *characterization of an optimized formulation of nanoparticles (NPs) loaded with a high content of dexamethasone palmitate (DEX-P), a chemotherapeutic adjuvant that decreases interstitial fluid pressure in tumors, and ^{111}In, a signaling agent, is described. These NPs are uniform in size and composition. Single photon emission computed tomography imaging demonstrates significant tumor uptake of ^{111}In-labeled DEX-P NPs in tumor-bearing mice. As with many nanoparticle-based drug delivery systems, significant liver accumulation is observed. Assessment of liver histology and blood tests show no apparent hepatic or renal toxicity of the DEX-P NPs. Conversion of DEX-P to DEX occurs when DEX-P NPs are incubated with mouse plasma, human tumor homogenate and ascites from tumor bearing mice, but not with human plasma. This conversion is slower in plasma from Es1$^{e(-/-)}$/SCID mice, a potential alternative animal model that better mimics humans; however, plasma from these mice are not completely devoid of esterase activity. The difference between blood and tumor esterase activity in humans facilitates the delivery of DEX-P NPs to tumors and the release of dexamethasone by an esterase trigger.*

Dr. J.-K. Kim, Dr. Y.-T. Yang, Prof. M. Jay
Division of Molecular Pharmaceutics
Center for Nanotechnology in Drug Delivery
Eshelman School of Pharmacy and Lineberger Comprehensive Cancer Center
University of North Carolina at Chapel Hill
Chapel Hill, North Carolina 27599, USA

Dr. J.-K. Kim
College of Pharmacy
Hanyang University
Ansan, Gyeonggi, 426-791, Republic of Korea

Prof. H. Yuan, Dr. J. Nie
Department of Radiology
University of North Carolina at Chapel Hill
Chapel Hill, North Carolina 27599, USA

Prof. M. Leggas
Department of Pharmaceutical Sciences
College of Pharmacy
University of Kentucky
Lexington, Kentucky 40506, USA

Prof. P. M. Potter
Department of Chemical Biology and Therapeutics
St. Jude Children's Research Hospital
Memphis, Tennessee 38105, USA

Prof. J. Rinehart
Department of Medicine
University of Kentucky
Lexington, Kentucky 40506, USA

Prof. M. Jay
Joint Department of Biomedical Engineering
University of North Carolina at Chapel Hill/North Carolina State University
Chapel Hill, North Carolina 27599, USA

Prof. X. Lu
Department of Pharmaceutical Sciences
School of Pharmacy
University of Connecticut
Storrs, Connecticut 06269, USA
Email: xiuling.lu@uconn.edu

DOI: 10.1002/smll.201200437

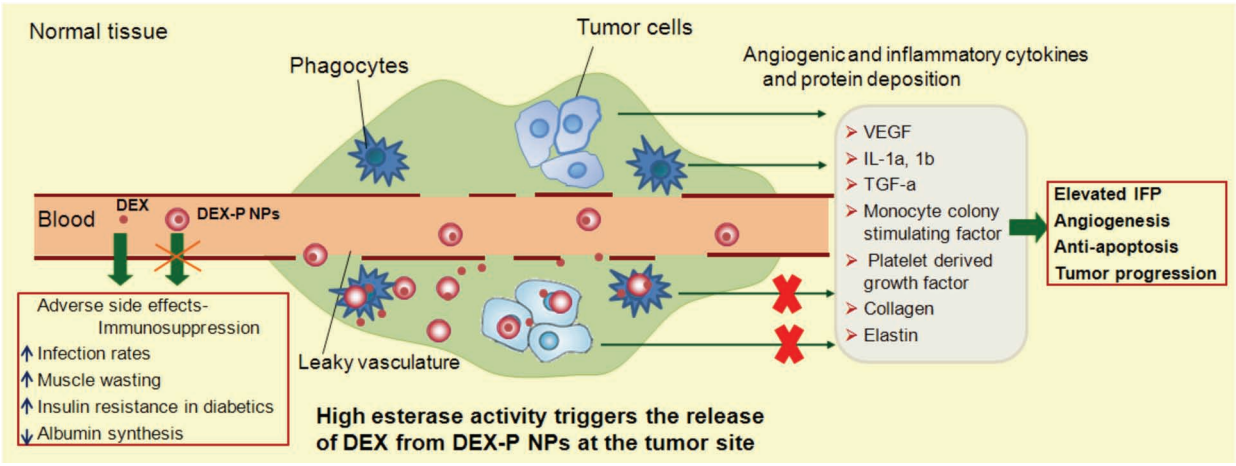

Figure 1. Theoretical model depicting the role of DEX-P NPs in blocking immune and cytokine related effects in the tumor and normal tissues. DEX will be released intra- and intercellularly and be taken up by phagocytes and tumor cells.

1. Introduction

There is a large unmet need to improve the therapeutic efficacy of cancer chemotherapeutic agents in solid tumors and to reduce their toxicities. One way this can be achieved is to reduce physiological barriers in the microenvironment of the tumor and thereby facilitate the uptake of these agents in tumors. Our previous studies demonstrated that the glucocorticoid dexamethasone (DEX) acts to enhance the effectiveness and reduce the toxicity of chemotherapeutic agents.[1,2] DEX appears to inhibit formation of high molecular weight proteins in tumor interstitial fluid space; these proteins increase colloidal osmotic pressure and thus elevate interstitial fluid pressure (IFP).[3–5] Tumor cells can often evade immune responses by releasing chemokines and cytokines that alter immune cell function, but this is more pronounced within the tumor microenvironment. This is typically observed in the form of macrophages being transformed from phagocytic type cell to a cell that accumulates in the tumor and releases proangiogenic and other molecules that facilitate tumor growth. Corticosteroids reduce cellular synthesis of multiple inflammatory and angiogenic cytokines such as vascular endothelial growth factor (VEGF), interleukin (IL)-1α, IL-1β, platelet derived growth factor (PDGF), transforming growth factor-alpha (TGF-α), monocyte colony stimulating factor (M-CSF aka CSF-1) and many others.[6–8] However, corticosteroids such as DEX also induce side effects, most notably suppression of the adaptive immune response due to depletion and inhibition of T cells.[9,10] Systemic delivery of DEX in cancer patients may cause serious adverse effects resulting in increased infection rates, increased muscle wasting, decreased albumin synthesis and increased insulin resistance in diabetics, thereby limiting its application in the clinic.

To reduce DEX systemic toxicity and maximize the previously reported synergistic effect of chemotherapy along with systemic DEX,[1,2] we have developed solid lipid nanoparticles (NPs) containing the palmitate ester of DEX (DEX-P) for augmented tumor delivery. In addition, DEX-P NPs as a chemotherapeutic adjuvant may improve the effectiveness of multiple anticancer drugs. Instead of developing an individual carrying system for a single anticancer drug, this pretreatment can be universal for improving the outcome of anticancer therapy.[11] Increased circulation retention times can be accomplished by 'pegylating' NP surfaces which reduces their interaction with circulating cellular elements and subsequent removal by cells of the reticuloendothelial system. The NPs accumulate in tumor tissue due to the enhanced permeability and retention (EPR) effect. Our previous *in vitro* studies indicated that the release of DEX from NPs in the tumors is by an enzymatic trigger, *i.e.*, esterases, which are present with high activity in tumors but with low activity in human plasma.[12,13] Carboxylesterases are over-expressed in tumor cells, and cell lysis can result in significant activity of this enzyme in interstitial fluid. These enzymes can convert DEX-P to DEX and subsequently release DEX at the tumor site which can then be taken up by inflammatory and tumor cells known to have surface glucocorticoid receptors for DEX.[14] Intact NPs containing DEX-P can also be taken up by phagocytes and tumor cells where the DEX-P is converted to DEX by esterases within the cells. Therefore, it may be not necessary to design NPs with tumor-specific targeting ligands on their surface. Our vision of the role that DEX-P NPs administration will have on the tumor microenvironment is depicted in **Figure 1**.

In this study, we attached ^{111}In on the surface of DEX-P NPs in order to image the biodistribution and tumor uptake of the NPs *in vivo* using single photon emission computed tomography (SPECT). These images can be used to calculate the delivered dose and for subsequent pharmacokinetic-pharmacodynamic modeling. The bioresponsive triggered release of DEX from DEX-P NPs has great clinical potential, but several challenges remain in the development and evaluation of such a system. The first is to prepare high payload NPs of uniform composition and properties. We previously reported that some formulations can lead to multiple populations of solid lipid nanoparticles where the drug payload in the different NP populations was not uniform.[15] The second

small NANO MICRO

challenge is to develop a proper animal model that can best mimic the human situation. High esterase activity in mouse plasma rapidly converts the ester prodrug DEX-P to DEX which can then be released from NPs. This is not expected to occur in human plasma due to its nominal esterase activity. The purpose of this study was to characterize the optimized NP formulation with a high DEX-P payload, track their tumor accumulation *in vivo* by imaging, and to determine if the pharmacokinetic profile of radiolabeled NPs was different in carboxylesterase-deficient athymic (*Es1*$^{e(-/-)}$/SCID) mice compared to athymic nude (nu/nu) mice, which are commonly used for human tumor xenograft and mimic humans for assessing anti-tumor efficacy *in vivo*.

2. Results and Discussion

2.1. Preparation of Radiolabeled High Payload DEX-P Nanoparticles

To increase the potency of nanoparticle-based drugs and reduce the potential side effects caused by the components of the nanocarriers, a high payload NP formulation is critical. In our previous study, when nanoparticles with a lipid to drug ratio of 10:1 (w/w) were prepared, two populations of nanoparticles with differing drug content were identified by gel filtration chromatography (GFC).[15] Thus, a new formulation was developed by substituting a portion of the lipid component with DEX-P so that the final lipid to drug (strearyl alcohol (SA) to DEX-P) ratio was 1:1 (w/w), with equivalent lipid to active drug (DEX) ratio of 1: 0.6. The mean particle size of these nanoparticles was 108.3 ± 1.3 nm with a narrow size distribution based on signal intensity by dynamic light scattering (polydispersity index = 0.146 ± 0.030). The addition of DMPE-DTPA to the formulation resulted in nanoparticles (DTPA-NPs) with a slightly larger particle size (115.0 ± 0.9 nm; polydispersity index = 0.172 ± 0.009). While measurement of intensity-based size distribution by dynamic light scattering is commonly reported for characterization of nanoparticles, this may be misleading if the system is heterogeneous. A new technology called nanoparticle tracking analysis was used to measure the number-based size distribution of these nanoparticles and revealed that the majority of our nanoparticles had a diameter of ~95 nm with a smaller population of particles of ~180 nm in diameter (**Figure 2**A). After passing [^{3}H]-DEX-P/[^{14}C]-stearyl alcohol nanoparticle preparation through a 0.2 μm filter, the recovery of radioactivity in the filtrate was 94.0% and 96.5% for ^{3}H and ^{14}C, respectively. The encapsulation efficiency of [^{3}H]-DEX-P was determined to be 91.7% after purification by ultrafiltration. The active drug loading (DEX to total NP mass) was calculated to be 6% based on the encapsulation efficiency, assuming no loss of other ingredients during the purification. In parallel, after passing through a 0.2 μm filter, the nanoparticle suspension was loaded onto a GFC column. The GFC profile of DTPA-NPs without radioactive metals bound to their surface yielded a single peak containing both DEX-P and SA, indicating that there was only one population of nanoparticles in the suspension (Figure 2B).

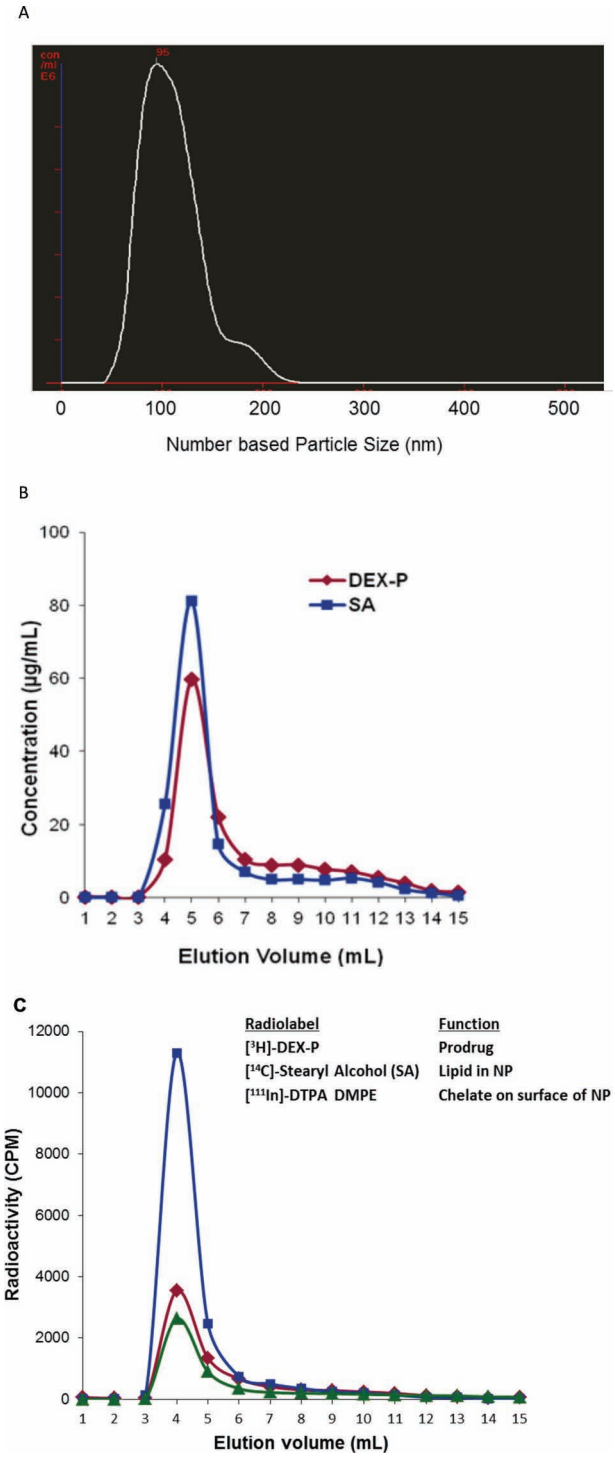

Figure 2. Number-based particle size distribution determined by nanoparticle tracking analysis (A) and GPC profiles of [^{3}H]-DEX-P loaded [^{14}C]-NPs (B) and [^{3}H/^{14}C/^{111}In]-NPs (C)

Radionuclides such as ^{111}In can be attached to nanoparticles by chelation with DTPA moieties and used for tracking the nanoparticles *in vivo* by noninvasive imaging. ^{111}In decays by electron capture and the distribution of ^{111}In-labeled NPs in animals can be imaged by SPECT. It has relatively long half-life (2.8 days), which is an advantage when

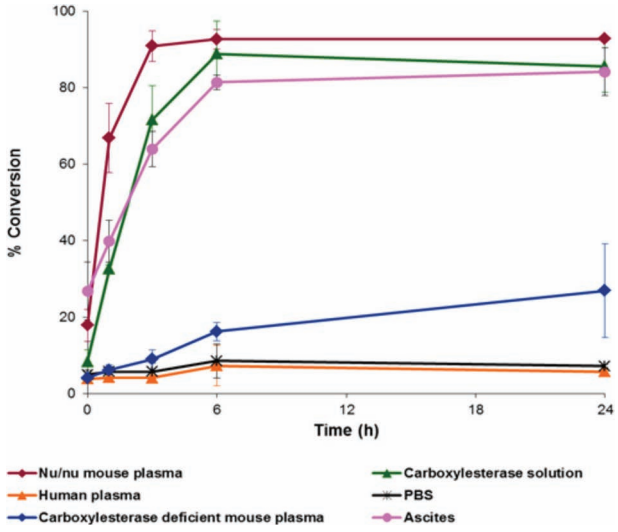

Figure 3. Conversion rate of NP associated DEX-P to DEX in various media

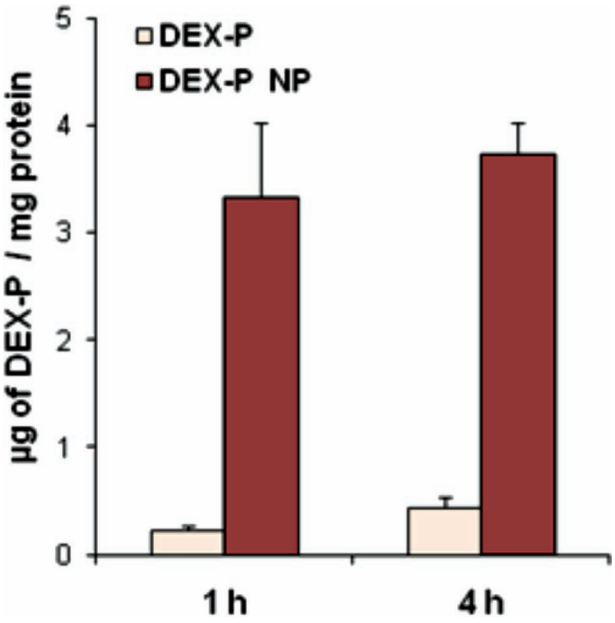

Figure 4. Uptake of DEX-P by A549 lung cancer cells after 1 h and 4 h incubation. [^{3}H]-DEX-P was used to quantify the mass of DEX-P in the cells. Cell protein concentration was determined by the BCA assay.

tracking nanoparticle biodistribution is required for more than 24 h. After chelation of the radioactive metals by DTPA on the surface of NPs, ultrafiltration was used to remove the unchelated metals. The recovery of the radioactivity from ultrafiltration was about 98%, indicating minimal membrane binding of the radiolabel. The GFC of purified [^{3}H]-DEX-P/[^{14}C]-SA/[^{111}In]-DTPA-NPs ([^{3}H/^{14}C/^{111}In]-NPs) showed that all three of these radionuclides were detected in a single peak indicating a mono-distribution particle size and composition of these nanoparticles (Figure 2C).

2.2. Conversion of DEX-P to DEX in Various Media

The rate at which NP-associated DEX-P is converted to DEX after incubation in various media is shown in **Figure 3**. In plasma from nu/nu mice, the conversion of DEX-P to DEX occurred immediately after incubation and was nearly 90% complete after 3 h. [^{3}H]-DEX conversion was also observed when the [^{3}H]-DEX-P NPs were incubated with a carboxylesterase solution (10 mg/mL), but the initial rate was slower than observed in nu/nu mouse plasma. When the NPs were incubated in human plasma, the conversion of [^{3}H]-DEX showed no significant difference from that in PBS ($p > 0.05$), while incubation in plasma from esterase-deficient mice showed significantly less conversion ($p < 0.05$) of [^{3}H]-DEX than observed in nu/nu mouse plasma. Modification of the NP formulation produced little effect on the esterolysis of DEX-P. It is expected that DEX-P will be stabilized in NPs in circulation in humans but not in mice. Both human tumor homogenate and tumor cell lysate exhibited high esterase activity as shown in our previous study.[12] Esterases are mainly expressed intracellularly by tumor cells and inflammatory cells, but tumor interstitial fluid may also have a high esterase content due to leakage from intact or damaged cells coupled with a defective drainage system to remove them from the interstitial space. Ascites due to cancer may reflect the properties of interstitial fluid. The conversation of DEX-P to DEX was tested in ascites from mice bearing human ovarian tumor. As shown in Figure 3, the conversation in ascites was comparably high to mouse plasma and esterase solution at each time point, which indicated that the drug may be released from NPs at both the intra- and inter- cellular level.

2.3. Tumor Cell Uptake

The uptake of nanoparticle-based DEX-P by tumor cells was 15 times greater than the uptake of free DEX-P after a 1 h incubation (**Figure 4**), although the uptake of the latter increased slightly after a 4 h incubation. However, there was no significant difference ($p > 0.05$) in the tumor cell uptake between the 1 h and 4 h incubation times for DEX-P NPs. Thus, it appears that nanocarriers may enhance the delivery of drug to the cells through internalization but may not affect uptake of free drugs by a diffusion mechanism.

2.4. SPECT/CT Imaging of ^{111}In-NPs

Non-invasive micro-SPECT imaging allows tracking of radiolabeled nanoparticles at different time points in the same animal after administration of radiolabeled NPs to avoid variation between animals. The distribution of the radioactivity in the animal can be related to anatomy by combining SPECT with computed tomography (CT). DMPE-DTPA, a phosphate ester lipid-based DTPA chelator was used to chelate ^{111}In for micro-SPECT/CT imaging. Because DEX-P exhibited varying stability in plasma from various species, it appears that the usual mouse models are inadequate predictors of ester

small NANO MICRO

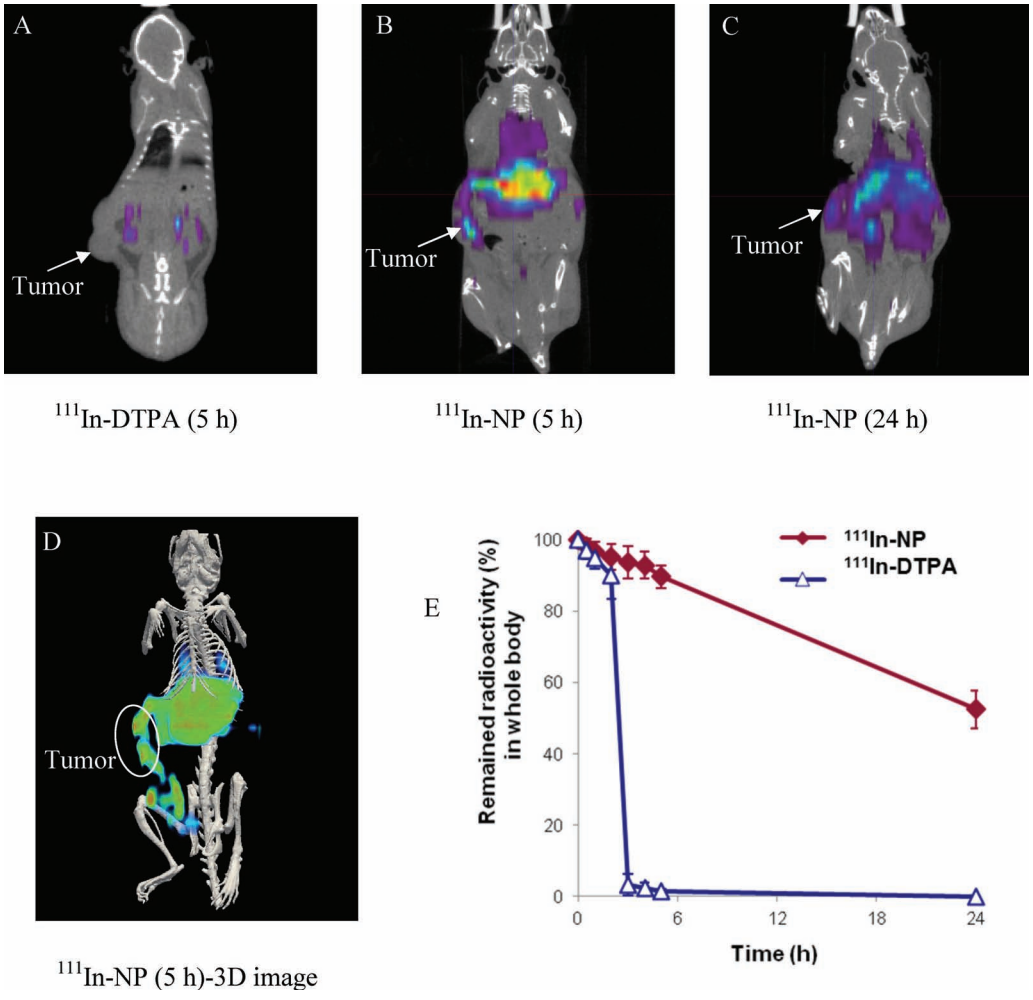

Figure 5. SPECT/CT images of tumor bearing mice. A,B and C are coronal SPECT/CT images 5 h after administration of ^{111}In-DTPA as well as 5 h and 24 h after administration of ^{111}In-NPs. The gray outline of the animal is seen in the CT image while the colored areas are the co-registered SPECT image of the ^{111}In distribution. A 3D volume rendering image is shown in D. These images show that the radioactivity associated with ^{111}In-NPs accumulates in the tumor region (along with significant liver accumulation) while radioactivity associated with ^{111}In-DTPA does not. E shows the whole body retention of radioactivity following administration of ^{111}In-NPs and ^{111}In-DTPA.

prodrug stability in humans. We were interested to learn if this phenomenon was also observed for other ester-linked compounds such as DMPE-DTPA. Therefore, [^{111}In]-DTPA was mixed with mouse plasma to determine if this radiolabel was bound by plasma protein. The recovery of ^{111}In from the ultrafiltrate was >90% indicating that ^{111}In remained bound to DTPA. The measured release of [^{111}In]-DTPA from the [^{111}In]-DTPA-NPs at 2 and 24 h time points was 1.1 ± 0.1% and 14.5 ± 0.7%, respectively, which was much slower than the release of [^{3}H]-DEX-P from NPs as previously reported.[12] DMPE-DTPA has two ester bonds and only when both are cleaved will the DTPA-metal complex be released from NPs. It is also possible that the ester bonds of DMPE-DTPA are more embedded within the NPs and are not readily accessible to the plasma esterases. The results indicated that DMPE-DTPA would not be rapidly hydrolyzed in the circulation even though DMPE and DTPA are linked by an ester bond, similar to DEX-P. In humans, the stability of the chelator is not expected to be an issue. Therefore, [^{111}In]-DTPA-NPs were used for the initial micro-SPECT/CT imaging study to determine the NP biodistribution in tumor-bearing nu/nu mice. A small molecule complex, [^{111}In]-DTPA, was administered intravenously as a control. Significant tumor as well as liver uptake was observed 5 h and 24 h after dosing [^{111}In]-DTPA-NPs (**Figure 5**B and 5C). This is particularly evident in the 3D volume rendering image from the 5 h time point (Figure 5D). Residual whole body radioactivity in these animals was as high as 55% after 24 h which indicated that the NPs have a long retention time (Figure 5E). In contrast, there was no tumor uptake and very little residual radioactivity in the whole animal 5 h after administration of [^{111}In]-DTPA (Figure 5A and 5E). These results are consistent with the *in vitro* study on the stability of ester bond of [^{111}In]-DTPA-NPs in mouse plasma.

Tumor and liver uptake of the [^{111}In]-DTPA-NPs was quantified from SPECT images. Tissue uptake of radioactivity based on region of interest (ROI) analysis was 1230.2 and 3533.8 counts/mm^3 in tumor and liver, respectively at the 5 h

Table 1. Plasma test of tumor bearing mice after i.v. injection of saline (control) or DEX-P NPs at 5 h and 1 week post injection (n = 4).

Average	BUN (mg/dL)	ALT (IU/L)	Alb (g/dL)	AST (U/L)	ALP (U/L)	LDH (U/L)	GGT (U/L)
Control	25.0 ± 7.1	36.7 ± 4.6	1.8 ± 0.1	74.0 ± 7.1	66.0 ± 7.1	776.0 ± 80.6	6.0 ± 0
5 h	23.0 ± 2.8	48.0 ± 3.7	2.4 ± 0.1	216.0 ± 101.7	71.2 ± 3.8	3243.5 ± 2293.2	4.0 ± 1.6
1 week	23.0 ± 2.2	36.2 ± 3.1	2.1 ± 0.2	72.3 ± 8.5	68.5 ± 5.3	699.0 ± 63.0	5.5 ± 1.0

time point, and both decreased after 24 h (485.6 and 1155.6 counts/mm^3 in tumor and liver, respectively, decay corrected). The intensity ratio of tumor to liver radioactivity signal from the images increased from 0.35 to 0.42 from the 5 h to the 24 h time point. The significant accumulation of the [^{111}In]-DTPA-NPs in the tumor as seen in the SPECT images indicated that this nanocarrier is capable of delivering DEX-P to tumors and that the concentration of DEX in the tumors can be quantified. [^{111}In]-DTPA NPs without DEX-P were also injected to tumor bearing mice to investigate the effect of the drug on the biodistribution. Tissues were collected at 24 h post injection.

2.5. Assessment of Toxicity

Significant liver accumulation of NPs was observed from SPECT images. To test the liver toxicity following administration of a single i.v. dose of DEX-P NPs containing 0.15 mg (the same dose as other *in vivo* studies) of DEX-P to tumor bearing mice, liver histology and blood tests were performed and compared to a saline control group. It appeared from the SPECT images that liver uptake was greatest 5 h after the administration compared to 2 h and 24 h time points (data was not shown). Thus, the 5 h and one week time points were chosen to study acute and delayed toxicity of the nanoparticles. Liver and kidney function were analyzed based on plasma tests including albumin (Alb), alanine transaminase (ALT), aspartate transaminase (AST), alkaline phosphatase (ALP), lactate dehydrogenase (LDH), gamma glutamyl transpeptidase (GGT) and blood urea nitrogen (BUN). No liver toxicity was identified 5 h and 1 week after the treatment based on liver histology. Mild-to-moderate vacuolation of convoluted tubules was observed in kidneys from both control and treatment groups, but the BUN test indicated normal renal function. **Table 1** shows that the AST, ALT and LDH levels increased 5 h after dosing DEX-P NPs in keeping with the known transient effect of glucocorticoids on hepatic enzymes.[16] However, no significant difference was found between the treatment group the control groups 1 week after administration (p > 0.05). For Alb, ALP, and GGT levels, no significant difference was observed between the treatment groups and the control group at both the 5 h and 24 h time points (p > 0.05). The results demonstrated that administration of DEX-P NPs did not result in liver or kidney toxicity despite high liver uptake.

2.6. Pharmacokinetics (PK) of NP-based DEX and ^{111}In-NPs

Due to the high esterase activity in mouse plasma, the nu/nu mouse may not be an appropriate animal model to mimic humans.[12,13] *Es*1$^{e(-/-)}$/SCID mouse model was used to determine if its reduced serum esterase activity, as demonstrated in the *in vitro* studies described above, affected the PK of NP-based DEX-P. The PK of [^{3}H]- DEX-P NP in nu/nu and *Es*1$^{e(-/-)}$/SCID mice, determined by tracking the radioactivity in blood, showed significant differences at early time points up to 3 h (**Figure 6**). The % of the injected dose per gram (%ID/g) of blood for the nu/nu mice were 4.43 ± 0.82, 1.49 ± 0.21 and 1.12 ± 0.23 at the 10 min, 30 min and 1 h time points, respectively, while the corresponding values for the *Es*1$^{e(-/-)}$/SCID mice were 7.64 ± 0.33, 2.58 ± 0.21, 1.86 ± 0.28. However, the *Es*1$^{e(-/-)}$/SCID mice apparently are not completely devoid of esterase activity, and enzymes other than carboxylesterase may cleave DEX-P as well. The free DEX released from the NPs is expected to be rapidly removed from the circulation. The PK curves of the two animal models were superimposable after 3 h. Furthermore, as shown in Figure 6, blood concentration of NPs in nu/nu mice as indicated by ^{111}In was significantly higher than blood concentration of [^{3}H]- DEX-P in nu/nu or *Es*1$^{e(-/-)}$/SCID mice (p < 0.05). This supported the speculation that the residual esterase activity in *Es*1$^{e(-/-)}$/SCID mouse plasma alters the biodistribution profile of the ester prodrug. However, this would not be the case in human plasma. The *in vitro* release data suggested that in humans the drug will be stabilized in the nanoparticles in circulation but will release DEX at the tumor site due to the local high esterase activity. Enhanced tumor delivery of nanoparticles was demonstrated by SPECT imaging. All the evidence suggested that DEX-P NP will enhance the delivery of DEX to tumors, while an appropriate animal model is needed to directly demonstrate this enhanced delivery to tumors.

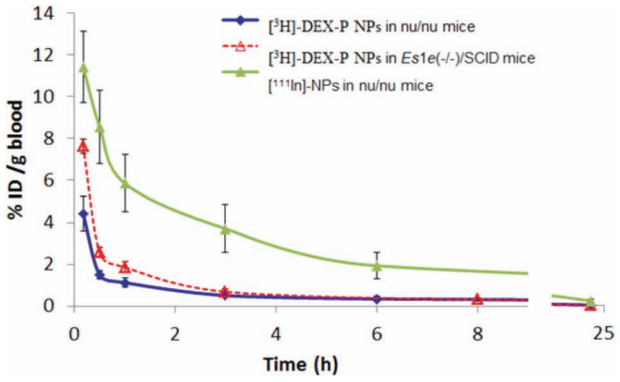

Figure 6. Pharmacokinetics (% of the injected dose per gram (%ID/g) *vs*. time) of [^{3}H]- DEX-P NPs and ^{111}In-NPs in nu/nu and *Es*1$^{e(-/-)}$/SCID mice.

small NANO MICRO

3. Conclusion

High payload nanoparticles containing a DEX ester prodrug, DEX palmitate, and an imaging agent, lipid DTPA chelated ^{111}In, were developed for delivering DEX specifically to tumors and tracking nanoparticles by SPECT. These dual therapeutic-imaging NPs were of uniform size and composition. Enzymatically-catalyzed esterolysis resulted in the release of DEX from the nanoparticles. Mouse models may not be appropriate for *in vivo* studies of ester prodrugs due to the high esterase activity in mouse plasma which was not observed in human plasma. High esterase activity in human tumors facilitates the triggered release of DEX specifically in tumors. The release can be in tumor cells, inflammatory cells or tumor interstitial space. SPECT/CT images showed significant tumor accumulation of NPs 5 h after intravenous administration of the [^{111}In]-DEX-P NPs to nu/nu mice bearing human lung cancer A549 tumors. Liver uptake dominates the tissue distribution of drug loaded NPs. However, no liver toxicity was observed based on liver histology and liver function tests. The DEX-P ester was hydrolyzed slower in plasma from *Es1*$^{e(-/-)}$/SCID mice. Blood concentrations of radioactivity were 2-fold higher in these mice within 3 h after i.v. injection of radiolabeled DEX-P NPs than in nu/nu mice. However, *Es1*$^{e(-/-)}$/SCID mice apparently are not completely devoid of esterase activity. This residual esterase activity may alter the biodistribution profile of the ester prodrug and, as a result, the PK profile of the tritium-labeled compounds is significantly different from that of ^{111}In-NPs. Further efforts are being made to develop an appropriate animal model that can demonstrate the efficacy of nanoparticle-based DEX-P delivery and bioresponsive release of DEX in tumor tissues. The use of a nanoparticle-based chemotherapeutic adjuvant for making the tumor microenvironment more favorable for anti-cancer drugs and thus improving the therapeutic indices of multiple therapeutic agents should be readily translatable to the clinic. Radiolabeled drug-containing NPs may be used in image guided drug delivery and be applied to the development of personalized medicine through pharmacokinetic-pharmacodynamic modeling.

4. Experimental Section

Materials: Tritiated dexamethasone ([6,7-^{3}H(N)]; [^{3}H]-DEX, specific activity = 35-50 Ci/mmol) and ^{14}C-stearyl alcohol ([1-^{14}C]; [^{14}C]-SA, specific activity = 50-60 mCi/mmol) were purchased from American Radiolabeled Chemicals Inc. (St. Louis, MO, USA). $^{111}InCl_3$ in HCl was purchased from PerkinElmer (Waltham, MA, specific activity 380-415 Ci/mmol).Dexamethasone (DEX) and bovine liver esterase were purchased from Sigma (St. Louis, MO, USA). Stearyl alcohol (SA) was obtained from Spectrum Chemical (Gardena, CA, USA). Brij78 and polysorbate 60 were provided by Croda Inc. (Edison, NJ, USA). Polyethylene glycol 6000 monostearate (PEG6000MS) was a gift from Hallstar (Chicago, IL, USA). 1,2-dimyristoyl-sn-glycero-3-phosphoethanolamine-N-diethylenetriaminepentaacetic acid (DMPE-DTPA) was purchased from Avanti Polar Lipids (Alabaster, AL, USA). Sepharose CL-2B was obtained from GE Healthcare (Piscataway, NJ, USA). All other chemicals were of reagent grade and used without further purification.

Preparation of High Payload DEX-P Nanoparticles: All NPs were prepared using the 'nanotemplate engineering' technique. The procedures to synthesize radiolabeled DEX-P ([^{3}H]-DEX-P) and prepare DEX-P NPs have been previously described.[12,13] The formulation was improved by replacing a portion of the lipid with DEX-P to achieve a high drug/lipid mass ratio of unity. The chelating reagent, DMPE-DTPA was incorporated into the NPs for the purpose of attaching radionuclides to the surface of the nanoparticles. Briefly, solid lipid nanoparticles were derived from a microemulsion comprised of [^{3}H]-DEX-P and non-labeled DEX-P (1 mg/mL), [^{14}C]-SA and non-labeled SA (1 mg/mL), polysorbate 60 (0.5 mg/mL), Brij78 (3.5 mg/mL), PEG6000MS (3.5 mg/mL) and DMPE-DTPA (0.1 mg/mL). Addition of warm DI water (pH 7.4, 70 °C) to the melted mixture of oil, drug and surfactants yielded a microemulsion. After stirring in a 70 °C water bath for 1 h, the warm microemulsion was cooled to 25 °C resulting in the formation of NPs (or DTPA-NPs) containing [^{3}H]-DEX-P and [^{14}C]-SA. The nanoparticle suspension was purified using a 0.2 μm filter to remove large particles and an ultrafilter (MWCO 50 kD) to remove free surfactants, DMPE-DTPA and drug. The retentate was washed 4 times and resuspended in 0.15 M ammonium acetate buffer (pH 5.0). The amounts of [^{3}H]-DEX-P and [^{14}C]-SA in the NPs were quantified using a Tri-Carb 3110TR Liquid Scintillation Counter (LSC; PerkinElmer, Waltham, MA, USA).

For the preparation of radiolabeled NPs, a neat solution of $^{111}InCl_3$ was added to the DTPA-NP suspension and stirred at 300 rpm for 1 h at room temperature. These NPs were purified by ultrafiltration (MWCO 50 kD) after washing three times with saline. Radioactivity from these photon-emitting radionuclides in each filtrate was quantified with a Wizard^{2} Automatic Gamma Counter (PerkinElmer, Waltham, MA, USA) using the 173 and 247 keV energy windows associated with the decay of ^{111}In. [^{111}In]-DTPA-NPs without radiolabeled SA and DEX-P were prepared for *in vivo* SPECT/CT imaging.

Characterization of the prepared DEX-P NPs: Particle size distributions of the formed NP suspensions based on intensity from dynamic light scattering were measured using a Zetasizer Nano ZS (Malvern, Worcestershire, UK). Particle size number distribution was measured by nanoparticle tracking analysis using a NanoSight LM10 system (Nanosight, Wiltshire, UK). Gel filtration chromatography (GFC) of NPs or [^{111}In]-DTPA-NPs containing [^{3}H]-DEX-P and [^{14}C]-SA was performed by using a 100 × 10 mm column packed with Sepharose CL-2B (bed volume = 8 mL). Two hundred microliters of [^{3}H/^{14}C]-NPs were applied to a pre-equilibrated column and eluted with phosphate buffered saline (PBS, pH 7.4) at a flow rate of 30 mL/h. Fractions (1 mL) were collected, and radioactivity in 100 μL aliquots of each fraction was quantified by mixing with 5 mL of liquid scintillation cocktail and counting using the LSC. The corrected specific activities of [^{3}H]-DEX-P and [^{14}C]-SA were calculated by dividing radioactivity by total mass. The mass of DEX-P and SA in each fraction was calculated by dividing the amount of radioactivity in the fraction by the corrected specific activity.

Conversion of DEX-P to DEX: Thin layer chromatography (TLC) was used to quantify the cleavage of DEX-P to DEX in various media. Briefly, 2 μL of [^{3}H]-DEX-P solution in DMSO or 2 μL of the [^{3}H/^{14}C]-NP suspension were added to 18 μL of nu/nu mouse plasma, *Es1*$^{e(-/-)}$/SCID mouse plasma, human plasma, ascites fluid or a 10 mg/mL in PBS esterase solution (n = 3). A mixture of [^{3}H]-DEX-P and plasma or enzyme solution was incubated at 37 °C.

At t = 0, 1, 3, 6 and 24 h, 2 μL of the mixture were collected and mixed with 10 μL of acetonitrile. The mixture was centrifuged at 10,000 g for 10 min. The entire supernatant was loaded onto a silica TLC plate and developed using a mobile phase consisting of chloroform and ethyl acetate (7:3, v/v). After completion of TLC separation, each plate was cut into two sections. The section with R_f = 0 –0.2 was recorded as 'bottom' (indicating DEX), while the other section of the TLC plate was recorded as 'top' (indicating DEX-P). The top and bottom sections of the TLC plates were solubilized with 1 mL of Solvable™ followed by the addition of scintillation cocktail. The radioactivity of each sample was quantified by liquid scintillation counting. All experiments were performed in triplicate.

Tumor Cell Uptake: Human lung epithelial carcinoma A549 cells were employed to study the tumor uptake of nanoparticles. A549 cells were purchased from the American Type Culture Collection (Manassas, VA) and cultured in DMEM with 2 mM L-glutamine, antibiotics, and 10% FBS at 37 °C in a humidified atmosphere with 5% CO_2. The cultured cells were seeded in a 24-well plate at a density of 1×10^5 cells/well with 1 mL of growth media and incubated at 37 °C under 5% CO_2 for 24 h. Cell numbers were adjusted so that each well contained approximately 2×10^5 cells. After removing the cell culture media, 1 mL of serum-free media containing the radiolabeled nanoparticles or [^{3}H]-DEX-P solution was added to each well. [^{3}H]-DEX-P solution served as a control and the concentration of DEX-P was adjusted to be the same as that in the nanoparticles. Due to its low solubility, DEX-P was dissolved in DMSO and then diluted 10 times using culture media. Following incubation periods of 1 and 4 h, the cells were washed and rinsed with PBS to remove the non-internalized radiolabels. To each well, 300 μL of cell lysis buffer was added and the cells were subsequently incubated and mixed for 10 min on a rocker. A 200 μL aliquot of the cell lysate was analyzed by liquid scintillation counting and the remainder (~100 μL) was saved to determine the protein concentration by the bicinchoninic acid (BCA) assay.

Animal Xenograft Tumor Model: Female nu/nu mice (20–25 g; Charles River Laboratories, Wilmington, MA) and female *Es*1$^{e(-/-)}$/SCID mice (22-28 g) developed at the St. Jude Children's Research Hospital (Memphis, TN) were handled following the guidelines of an approved protocol by the University of North Carolina Institutional Animal Care and Use Committee in accordance with the NIH Guidelines. Human non-small cell lung epithelial carcinoma A549 cells were allowed to grow to 70% confluence and resuspended in DMEM medium after incubation with trypsin. Mice were injected with A549 cells (2×10^6 cells/100 μL/mouse) subcutaneously on the right flank. The tumors were measured by calipers twice per week and the tumor volume was calculated.

In vivo Imaging Study: Imaging of the biodistribution of [^{111}In]-DTPA NPs was conducted using a small animal SPECT/CT imaging system (eXplore speCZT/CT-120, GE Healthcare Inc., Waukesha, WI, USA). Female nu/nu mice bearing human lung carcinoma A549 xenografts were administered [^{111}In]-DTPA or [^{111}In]-DTPA-NPs containing DEX-P *via* tail vein (n = 6). Each mouse was administered approximately 0.5 mCi of ^{111}In in 150 μL of either saline (for [^{111}In]-DTPA) or NP suspension containing 0.15 mg of DEX-P. At various time points, the amount of radioactivity retained in the whole body of the mouse was measured using an ionization chamber/dose calibrator (Model CRC-15R, Capintec Inc., Ramsey, NJ, USA). SPECT/CT images were acquired at 5 and 24 h after administration of the radiolabel. Anatomical CT imaging was performed initially followed by SPECT imaging in which images were acquired using a mouse slit collimator providing 1.5 mm transaxial resolution and 2.5 mm axial resolution. The SPECT and CT images were co-registered and the liver and tumor volumes were manually segmented based on CT images. The average radioactivity counts of each voxel ($0.4 \times 0.4 \times 2.46$ mm^3) in liver and tumor tissues of the SPECT images were measured using MicroView software on reconstructed tomographic images.

Toxicity Assessments: Tumor bearing mice were injected *via* tail vein with either nanoparticles containing dexamethasone (150 μL of NP suspension containing 0.15 mg DEX-P) or saline as control (n = 4). Blood, liver, kidney and spleen were collected at 5 h and 1 week after the injection. Liver and kidney function were analyzed based on plasma tests including albumin (Alb), alanine transaminase (ALT), aspartate transaminase (AST), alkaline phosphatase (ALP), lactate dehydrogenase (LDH), gamma glutamyl transpeptidase (GGT) and blood urea nitrogen (BUN). Liver, kidney and spleen tissues were fixed by 10% formalin and embedded in paraffin. Tissue slices were subjected to hematoxylin and eosin (H&E) staining.

Pharmacokinetics of DEX-P and ^{111}In-NPs: The PK of ^{111}In-NPs and NP-based [^{3}H]-DEX-P was studied in nu/nu and *Es*1$^{e(-/-)}$/SCID mice bearing A549 tumors by obtaining blood samples at 15 min, 30 min, 1, 3, 6 and 24 h after administration and calculating%ID/g blood after measuring the radioactivity and the mass of the blood (n = 6 for nu/nu mice groups and n = 3 for *Es*1$^{e(-/-)}$/SCID due to the limited number of these mice available).

Statistical Analysis: Data are presented as mean ± standard deviation. Groups were compared using analysis of variance (ANOVA) one-way test with SigmaStat 3.5 software (Systat Inc., San Jose, CA). Differences were considered statistically significant when $p < 0.05$, and the Holm-Sidak method was used to perform pairwise multiple comparisons on significant effects and interactions.

Acknowledgements

The authors are grateful for financial support from Carolina Partnership, University Research Council, University of Cancer Research Fund as well as the Benedict Cassen Postdoctoral Fellowship from the Education and Research Foundation for the Society of Nuclear Medicine. We appreciate the help from the Small Animal Imaging Core and Image Analysis Core at the Biomedical Research Imaging Center (BRIC), University of North Carolina at Chapel Hill. Work in the Potter laboratory is supported by NIH grants CA108775, A Cancer Center Core grant CA21765 and by the American Lebanese Syrian Associated Charities and St Jude Children's Research Hospital (SJCRH).

[1] H. Wang, M. Li, J. J. Rinehart, R. Zhang, *Clin. Cancer. Res.* **2004**, *10*, 1633–1644.
[2] H.Wang, M. Li, J. J. Rinehart, R. Zhang, *Cancer Chemother. Pharmacol.* **2004**, *53*, 459–467.
[3] K. R. Cutroneo, *Int. J. Biochem. Cell Biol.* **2002**, *34*, 194–203.
[4] M. P. Gras, F. Verrecchia, J. Uitto, A. Mauviel, *Exp. Dermatol.* **2001**, *10*, 28–34.
[5] Y. Oishi, Z.W. Fu, Y. Ohnuki, H. Kato, T. Noguchi, *Br. J. Dermatol.* **2002**, *147*, 859–868.

small NANO MICRO

[6] C. H. Heldin, K. Rubin, K. Pietras, A. Ostman, *Nat. Rev. Cancer* **2004**, *4*, 806–813.
[7] G. Dranoff, *Nat. Rev. Cancer* **2004**, *4*, 11–22.
[8] M. M. Mueller, N. E Fusenig, *Nat. Rev. Cancer* **2004**, *4*, 839–849.
[9] D. Franchimont, J. Galon, M. Gadina, R. Visconti, Y. Zhou, M. Aringer, D. M. Frucht, G. P. Chrousos, J. J. O'Shea, *J. Immunol.* **2000**, *164*, 1768–1774.
[10] D. Franchimont, *Ann. N.Y. Acad. Sci.* **2004**, *1024*, 124–137.
[11] X. Lu, M. D. Howard, M. Mazik, J. Eldridge, J. J. Rinehart, M. Jay, M. Leggas, *AAPS J.* **2008**, *10*, 133–140.
[12] X. Lu, M. D. Howard, D. R. Talbert, J. J. Rinehart, M. Jay, M. Leggas, *AAPS J.* **2009**, *11*, 120–122.
[13] C. L. Morton, M. Wierdl, L. Oliver, M. K. Ma, M. K. Danks, C. F. Stewart, J. L. Eiseman, P. M. Potter, *Cancer Res.* **2000**, *60*, 4206–4210.
[14] Y. S. Lu, H. C. Lien, P. Y. Yeh, S. H. Kuo, W. C. Chang, M. L. Kuo, A. L. Cheng, *Lung Cancer* **2006**, *53*, 303–310
[15] J. K. Kim, M. D. Howard, T. D. Dziubla, J. J. Rinehart, M. Jay, X. Lu, *ACS Nano* **2011**, *5*, 209–216.
[16] E. R. Jackson, C. Kilroy, D. L. Joslin, S. J. Schomaker, I. Pruimboom-Brees, D. E. Amacher, *Drug Chem Toxicol.* **2008**, *31*, 427–45

Received: February 27, 2012
Revised: April 17, 2012
Published online: July 6, 2012